Proceedings of the XVII ECSMGE-2019
Geotechnical Engineering foundation of the future
ISBN 978-9935-9436-1-3

doi: 10.32075/17ECSMGE-2019-0692

XVII European Conference
ECSMGE 2019
Reykjavik
on Soil Mechanics
and Geotechnical Engineering

Modelling a gas flow experiment in Mx80 bentonite

Modélisation d'un essai d'écoulement de gaz dans la bentonite Mx80

I.P. Damians
International Center for Numerical Methods in Engineering (CIMNE) and Universitat Politècnica de Catalunya – BarcelonaTech (UPC), Barcelona, Spain

S. Olivella, A. Gens
Universitat Politècnica de Catalunya – BarcelonaTech (UPC), Barcelona, Spain

ABSTRACT: A gas injection test performed on compact bentonite was carried out at the British Geological Survey. The test is composed of two stages (i.e. hydration followed by gas injection). After gas breakthrough and a period of gas flow through the sample, the injection pump was stopped whilst stresses and pore pressures were continuously monitored. A 3D numerical model has been developed to simulate the gas injection test and to achieve similar gas pressure responses. After sensitivity analysis of the model, a satisfactory calibration approach was possible using both hydraulic and coupled hydro-gas-mechanical model assumptions.

RÉSUMÉ: Un essai d'injection de gaz, réalisés sur de la bentonite compacte, ont été effectués au British Geological Survey. L'essai est composé de deux étapes (l'hydratation suivie d'un essai d'injection de gaz). Après la percée du gaz et une période de gaz traversant l'échantillon, la pompe d'injection a été arrêtée tandis que les contraintes et les pressions interstitielle étaient surveillées en permanence. Un modèle numérique 3D a été développé pour simuler le test d'injection de gaz et obtenir des réponses similaires à la pression du gaz. Après des analyses de sensibilité du modèle, une approche satisfaisante de calibration fut rendu possible en utilisant des hypothèses de modèle hydraulique et couplé hydro-gaz-mécanique.

Keywords: Hydraulic 3D model; Gas flow; Mx80 bentonite

1 INTRODUCTION

A gas injection test performed on compacted Mx80 bentonite was carried out at the British Geological Survey. This experiment, designated as Mx80-D, represents the first test of a series of tests analyzed in Task A of the DECOVALEX project (Harrington *et al*. 2016, Daniels and Harrington 2017). Those tests are useful to increase the understanding of potential gas flow through these low permeability materials. With these tests it is possible to improve bentonite functionality (e.g., in nuclear waste repositories) and confirm its suitability for isolating spent fuel.

Figure 1 displays the testing cell apparatus with the main details of the instrumentation on the bentonite sample.

The Mx80-D test comprises two main stages: a hydration stage followed by helium gas injection. The injected gas pressure was fixed to 1 MPa from 7.3 to 39.3 days and to 3 MPa from 39.4 to 46 days. Afterwards, gas flow rate was continuously increased up to a constant flow rate value until a breakthrough point occurred (at

71.5 days). After breakthrough and a period of gas flow through the sample, the injection pump was stopped whilst stresses and pore pressures were continuously monitored at several monitoring point on the sample (see Figure 1) up to the end of the test at day 121.

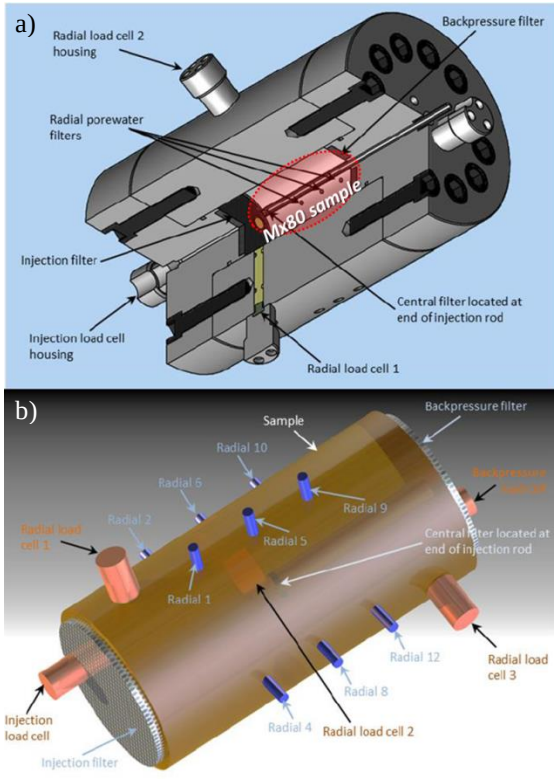

Figure 1. Mx80-D test: main details of pressure vessel (a) and Mx80 sample monitoring locations (b) (modified from Daniels and Harrington 2017).

2 MODELLING APPROACH

2.1 Conceptual model

A series of two phase flow calculations on a 3D geometry assuming porosity heterogeneity, which in turn produces heterogeneity of permeability and retention curve (exponential equation), were preliminary carried out. Boundary condition of prescribed gas flow and prescribed gas pressure allowed the performance of two alternative calculations with preliminary calibration performance where permeability and porosity values were first approximated (Damians *et al*. 2017). Comparison with measured values of inflow pressure and pressure at intermediate sensors was carried out.

Because actual material deformations produce changes in permeability and retention curve, coupled hydro-(gas)-mechanical modelling was then performed based on the previous description of heterogeneity and including elasticity. Finally, separate terms for matrix and fractures relative permeability model feature was then included in HM modelling, in addition to permeability heterogeneity with a fixed initial porosity and elasticity.

The primary variables were gas pressure and liquid pressure for the two phase flow model. Stress developments at several points were added for calculations coupled to mechanical. In addition, the individual components of helium mass flux at mid cross section of the sample were obtained. The conservation equations solved are the conservation of water mass, conservation of helium mass and stress equilibrium. As stated, deformation was modelled assuming elasticity with effective stress (fluid pressure as the maximum between gas and liquid) Permeability and retention curve were assumed to be a function of porosity.

CODE_ BRIGHT was used (Olivella *et al*. 1996) which is a FORTRAN FEM Code developed at Universitat Politècnica de Catalunya – BarcelonaTech (DECA-UPC) and International Center for Numerical Methods in Engineering (CIMNE).

2.2 Test geometry and initial boundary conditions

The entire 3D geometry was considered (see Figure 2). The domain was divided into small zones to which different initial properties were assigned. Model dimensions for the cylindrical sample test were considered according to specifications provided, which are: 120 mm-long ×

60 mm-diameter. In the model, 5 mm-thick filters were assumed on each side of the sample (i.e., injection and backpressure). The numerical domain discretization was performed with a 7917-nodded mesh and 7168 hexahedral elements.

Initial porosity with small heterogeneous distribution is assigned randomly to sub-zones (see Figure 2). This condition was maintained in the first two cases shown (hydraulic and hydro-mechanical with embedded permeability). In the third case (hydro-mechanical with embedded permeability and different relative permeability for matrix and fractures), as explained later, the initial porosity was assumed to be the same in all the soil volume (0.41) and the heterogeneity was considered using three different intrinsic permeability values with different affected volume weighting.

Constant pore pressure of 0.1 MPa assuming initially saturated sample was the initial condition for the flow equations. For the cases including mechanical modelling, an initial stress of 2 MPa was considered and the domain assumed to be at constant volume. 170 cm^3 of volume was considered at the injection.

Boundary conditions for the flow problem were divided into three types depending on whether the injection surface, the intermediate measuring points, or the back-surface was considered. As indicated above, either prescribed pressure or prescribed flow rate were considered on the injection surface, but results are presented for prescribed flow rate cases only, better fitting the test procedure where the gas pressure is actually caused by the flow rate.

2.3 *Material parameters*

From all models developed (several preliminary sensitivity analysis performed), the three following ones were selected to be included herein as the most representative ones. They represent three different conceptual approaches including different embedded permeability strategy, and, in addition, the resulting performance was in relatively good agreement with the measured results. The three models presented are: hydraulic model with two phase flow only, hydro-mechanical model (HM_1) assuming elasticity with combination of matrix and embedded fracture permeability (cubic law), and hydro-mechanical model (HM_2) assuming elasticity with combination of matrix and embedded fracture permeability (cubic law) and different relative permeability for matrix and fractures. The main features of the constitutive equations of these three models are presented in the following sections.

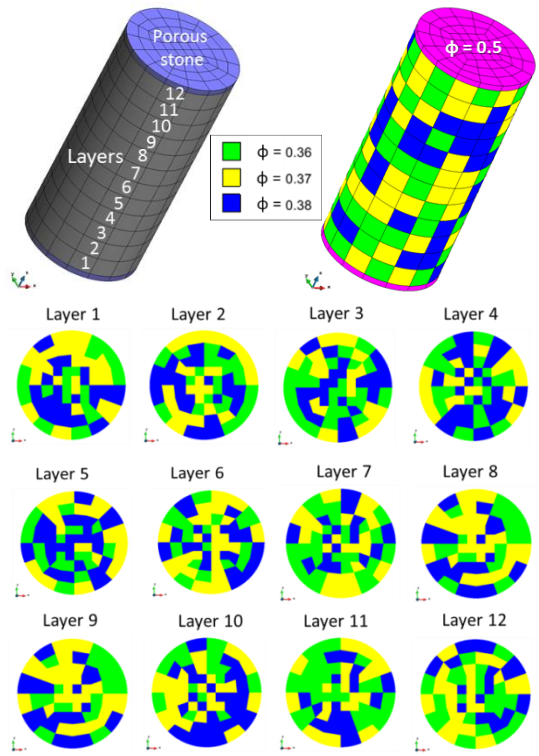

Figure 2. Layer-by-layer random porosity distribution (1/3 weighting each).

2.3.1 *Hydraulic model: two phase flow*

Material parameters for the Two-phase flow are presented in Table 1. The intrinsic permeability (k), defined as a function of porosity (ϕ), is calculated as follows:

$$k = k_0 \exp(b_k(\phi - \phi_0)) \quad (1)$$

where k_0, ϕ_0, and b_k are parameters (see Table 1). Porosity only changes in space and is heterogeneously and randomly distributed with the values 0.36, 0.37, and 0.38 with a 1/3 weighting each (see Figure 2).

The retention curve is defined by the following equation:

$$S = \left(1 + \left(\frac{P_g - P_l}{P_{VG}}\right)^{\frac{1}{1-\lambda_{VG}}}\right)^{-\lambda_{VG}} \quad (2)$$

where P_g, P_l are the gas and liquid pressures according to Van Genuchten model; λ_{VG} is the shape function; P_{VG} is the capillary pressure Van Genuchten parameter, calculated as:

$$P_{VG} = P_{VG,0} \exp(b_{VG}(\phi_0 - \phi)) \quad (3)$$

where $P_{VG,0}$ and b_{VG} are parameters, defined in Table 1. As indicated above, porosity only changes in space and is heterogeneously distributed. Relative permeability (k_r) is a function of the degree of saturation (S_α), as:

$$k_{r\alpha} = S_\alpha^{\,n_\alpha} \Rightarrow \begin{cases} k_{rl} = S_l^{\,n_l} \text{ (liquid)} \\ k_{rg} = S_g^{\,n_g} \text{ (gas)} \end{cases} \quad (4)$$

Table 1. Material properties for hydraulic H model:

Parameters	**Soil (Mx80 bentonite)**		
Initial porosity, ϕ_0:	0.36	0.38	0.39
Intrinsic permeability: k_0 / b_k	5.6×10^{-18} / 60		
Water retention curve, $P_{VG,0}$ / λ_{VG} / b_{VG} :	27 / 0.45 / 33		
Rel.perm. n_g / n_l (power):	3 / 3		

2.3.2 Hydro-mechanical model HM_1

This model assumed elastic mechanical behavior and a combination of matrix and embedded fracture permeability (cubic law). Figure 3 presents a conceptual representation of the embedded permeability model. A single fracture characterized by its aperture *b* (Fig.3-left) and a finite element diagram with a series of parallel fractures (Fig.3-right). The width of the element is *s*, the aperture of the fractures is *b*, the associated width to each fracture is *a* (which is equivalent to spacing between fractures), and the number of fractures in the element is *n*.

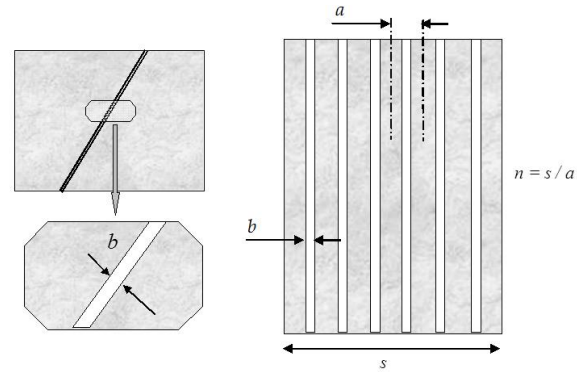

Figure 3. Embedded permeability model: Conceptual diagram representation (Olivella and Alonso 2008).

Intrinsic permeability is a function of material matrix porosity (k_{matrix}) and internal fracture aperture (k_{matrix}), as:

$$k = k_{matrix} + k_{fractures} \quad (5)$$

The matrix permeability component is computed as:

$$k_{matrix} = \frac{k_0(1-\phi_0)^2}{\phi_0^3}\frac{\phi^3}{(1-\phi)^2} \quad (6)$$

The permeability controlled by the internal fractures is defined as:

$$k_{fractures} = \frac{b^3}{12a} \quad (7)$$

where the aperture b is calculated as:

$$b = b_0 + (\varepsilon - \varepsilon_0)a \le b_{\max} \quad (8)$$

where ε and ε_0 refer to strain (with $\varepsilon > 0$ meaning extension), and b_0 and $b_{\max}$ are implicitly defined in the equations and in Table 2. From Eq. 5 and combining Equations 6 and 7, the following equation is obtained:

$$k = k_{matrix} + k_{fractures} = \frac{k_0(1-\phi_0)^2}{\phi_0^3}\frac{\phi^3}{(1-\phi)^2} + \frac{b^3}{12a} \quad (9)$$

Relative permeability (k_r) is a function of the degree of saturation (S_α), as in the previous case (see Equation 4),

The retention curve may change with the opening of fractures as pore size controls the gas entry values, and fractures may play the role of big pores leading to a reduction of gas entry value. The capillary pressure Van Genuchten parameter (P_{VG}) can then be calculated as:

$$P_{VG} = P_{VG,0}\sqrt[3]{\frac{k_0}{k}} \quad (10)$$

According to previous definitions, the actual model material zones (three different zones with the same porosity distribution as used in the previous hydraulic model) consider the hydraulic parameters presented in Table 2. With these parameters, the intrinsic permeability trends with regard to the associated internal fracture width (or fracture spacing) presented in Figure 4 are obtained.

The soil material stiffness was given by 100 MPa for shear (G) and bulk (K) moduli values.

2.3.3 Hydro-mechanical model HM_2

As commented, this model assumed elasticity together with a combination of matrix and embedded fracture permeability (cubic law) and different relative permeability for matrix and fracture:

$$k_g = k_{rg,m}k_m + k_{rg,f}k_f = S_g^n k_{matrix} + S_g k_{fractures} \quad (11)$$

Table 2. Material properties for HM_1 model:

Parameters	**Soil (Mx80 bentonite)**		
Initial porosity, ϕ_0 (-):	0.36	0.37	0.38
Intr.perm., k_0 (m^2):	2.2e-18	3.9e-18	7.1e-18
Spacing, a (m):	2.0e-5	9.5e-6	5.0e-6
Initial aperture, b_0 (m):	1.0e-8	1.0e-8	1.0e-8
Max.apert., $b_{\max}$ (m):	1.7e-6	1.3e-6	1.1e-6
Water ret.curve, $P_{VG,0}$ (MPa):	37.8	27.0	19.4
λ_{VG} (-):	0.45	0.45	0.45
Rel.perm., n_g / n_l (power):	3 / 3		

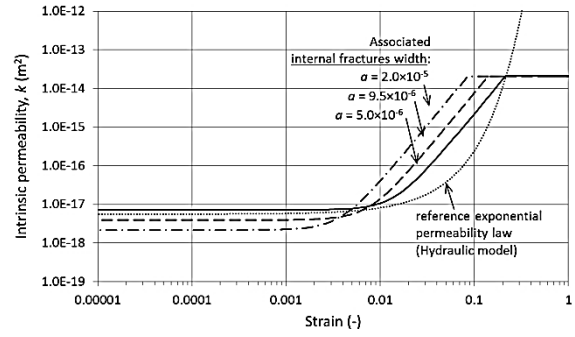

Figure 4. Material intrinsic permeability law: HM_1.

The previous model (HM_1) assumed the same relative permeability for both matrix and fractures (as intrinsic permeability is separated between matrix and fracture contributions, relative permeability is consequently split as well).

The hydraulic parametrical values presented in this case (HM_2) are shown in Table 3, leading to the intrinsic permeability trends presented in Figure 5. It should be noted that the initial porosity was assumed to be higher and equal to 0.41, and uniform in all the soil volume. Also a significantly lower permeability was assumed in this current HM_2 model case compared to the previous HM_1 model (order of magnitude 10^{-18}

for HM_1 and 10^{-19} for HM_2) better suiting the actual material features.

The soil material stiffness was given by an Elastic modulus E = 307 MPa, and Poisson's ratio v = 0.44, corresponding to a shear modulus G = 106.6 MPa and bulk modulus K = 852.8 MPa. Changes on deformability would imply changes on maximum fracture aperture values, as specified in Table 3.

Table 3. Material properties for HM_2 model:

Parameters	**Soil (Mx80 bentonite)**		
Initial porosity, ϕ_0 (-):	0.41	0.41	0.41
Intr.perm., k_0 (m^2):	2.2e-19	3.9e-19	7.1e-19
Spacing, a (m):	2.0e-5	9.5e-6	5.0e-6
Initial aperture, b_0 (m):	1.0e-8	1.0e-8	1.0e-8
Max.apert., b_{max} (m):	3.4e-7	2.7e-7	2.2e-7
Water ret.curve,			
$P_{VG,0}$ (MPa):	37.8	27.0	19.4
λ_{VG} (-):	0.45	0.45	0.45
Rel.perm., n_g / n_l (power):		2 / 3	

In order to avoid a too homogenous response of fluxes and to serve as seed for flow path formation, a heterogeneous field of permeability was incorporated in the HM_2 model case. As with the initial porosity in HM_1 model, a layer-by-layer randomly permeability distribution was assumed in the HM_2 model case, as shown in Figure 6, which corresponds to a 2/3 weighting distribution for the highest permeability value, and 1/6 weighting distribution for the lower permeability value (see Table 3).

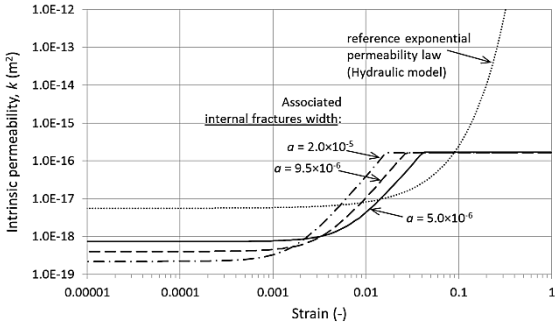

Figure 5. Material intrinsic permeability law: HM_2.

3 RESULTS

Results for two phase flow modelling are presented below compared with the two considered coupled hydro-mechanical models (cases H, HM_1, and HM_2).

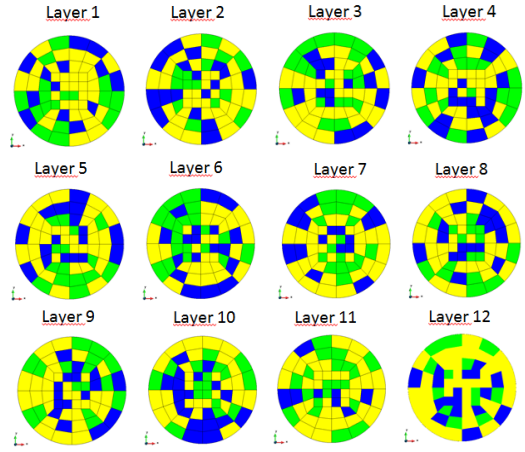

Figure 6. Layer-by-layer random permeability distribution assumed: 2/3 weighting for higher permeability value (yellow: k_0=2.2e-19 m^2) and 1/6 weighting for the lower values (blue and green, 3.9e-19 m^2 and 7.1e-19 m^2, respectively).

The proposed methodology provided results reasonably satisfactory with some pressure over prediction of the rigid two phase flow model. It was useful to find a combination of k_0 and n_g that leads to a pressure evolution similar to measurements which could be used as reference model for subsequent mechanical coupling calculations (Damians *et al*. 2017). Modelling gas injection tests using two phase flow in a rigid porous material was a preliminary step.

Inflow and outflow for both hydraulic and hydro-mechanical model results are presented in Figure 7.

Injection and back-pressure results are presented in Figure 8, and a reasonable agreement is obtained in all models.

Radial pore pressure results at the arrays are presented in Figure 9. Improved peak pressure values were obtained due to the mechanical implementation.

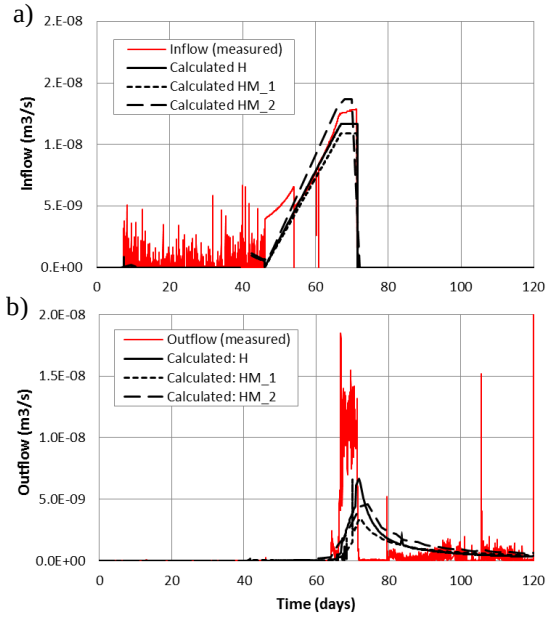

Figure 7. Inflow (a) and outflow (b) evolution results.

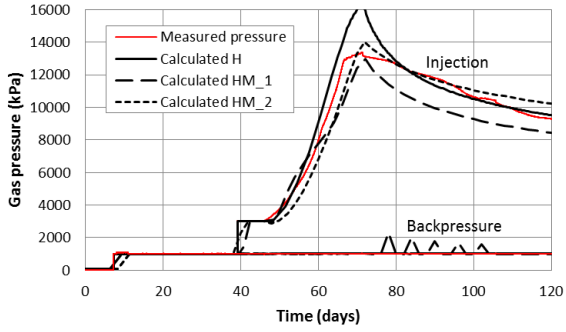

Figure 8. Injection and backpressure evolution results.

Figure 10 shows advective gas flux ($m^3/m^2/s$ = m/s) vectors example during injection at day 65 and after breakthrough (i.e., during dissipation) at day 75. The same vector scale is maintained to facilitate comparison. As expected, the larger flow-vector magnitudes occur at different locations before and after the breakthrough point.

Stress development at load cell locations data are presented in Figure 11 (for hydro-mechanical models).

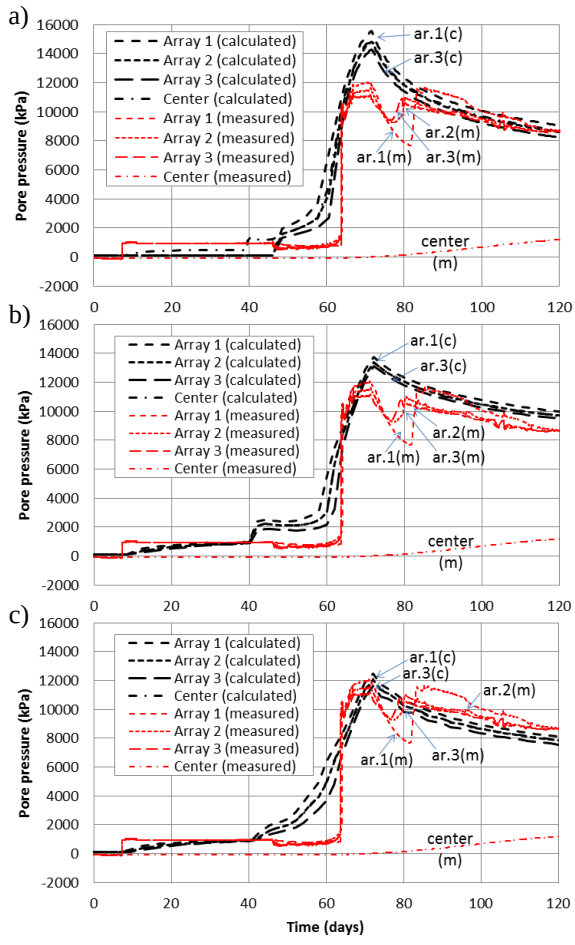

Figure 9. Pore pressure evolution results: Hydraulic model (a), HM_1 (b), and HM_2 (c).

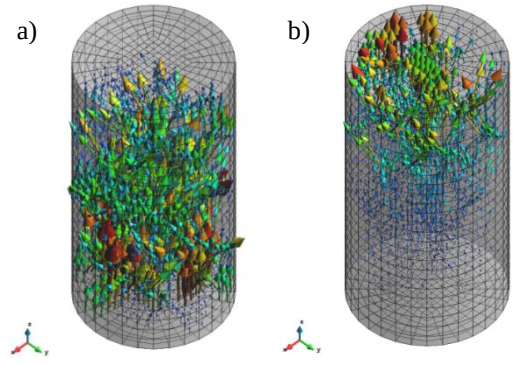

Figure 10. Advective gas flux at day 65 during injection (a) and day 75 during dissipation (b).

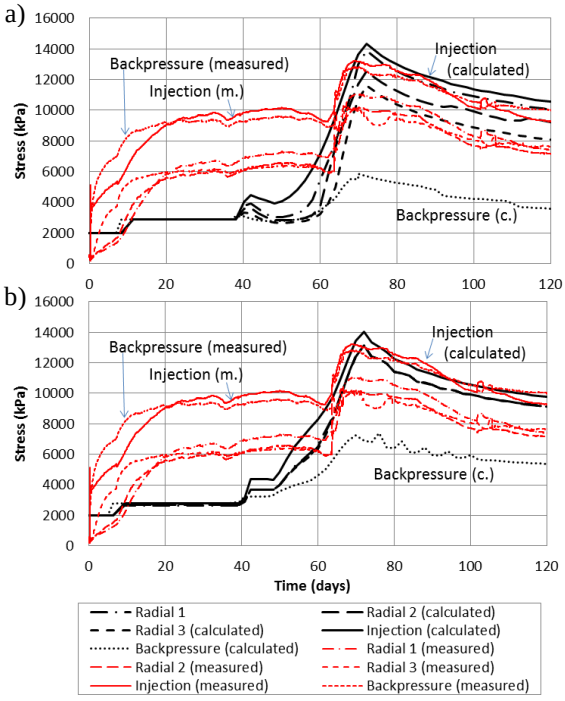

Figure 11. Stress evolution results (hydro-mechanical models): HM_1 (a) and HM_2 (b).

The mass gas flux evolution in the cross-section mid-plane of the sample is shown in Figure 12, in which the different flux components are plotted separately (i.e., helium diffusion/dispersion through liquid phase, advection helium flux due to liquid phase flow, and advection helium gas phase itself). It can be noted that the main helium mass flux contribution after the breakthrough is due to advection.

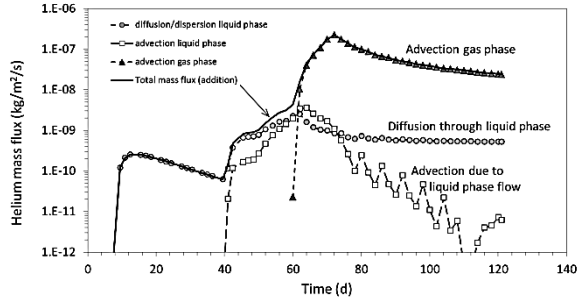

Figure 12. Evolution of the individual components of helium mass flux.

4 CONCLUSIONS

Despite the slight differences among model results, the proposed methodology provides predictions reasonably satisfactory under hydro-mechanical (embedded fracture permeability) modelling assumptions. It has been possible to find suitable combinations of k_0 (and n_g), and related embedded fracture spacing and aperture parameters leading to pressure evolution in good agreement with measurements. Further sensitivity calculations will permit better calibration and understanding.

5 ACKNOWLEDGEMENTS

The support provided by the National Radioactive Waste Management Agency, ANDRA (coordination by Jean Talandier) is greatly acknowledged. This is part of gas modelling research in DECOVALEX-2019 project (Task A coordinated by Jon Harrington and Elena Tamayo-Mas, British Geological Survey).

6 REFERENCES

Damians, I.P., Olivella, S., and Gens, A., 2017. Modelling gas flow experiments in Mx80 bentonite. *9th Workshop on CODE_BRIGHT*. UPC-BarcelonaTech, Spain, 23rd May 2017.

Daniels, K.A. and Harrington, J.F., 2017. The Response of Compact Bentonite during a 1D Gas Flow Test. BGS - OR/17/067. 19pp.

Harrington, J.F., R Cuss, C Graham, S, 2016. British Geological Survey, Radioactive Waste Management Limited, ENGINEER (modElliNg Gas INjection ExpERiments), DECOVALEX 2019, Specs. for Task A.

Olivella, S. and Alonso, E.E., 2008. Gas flow through clay barriers. *Géotechnique* **58**: 157-168.

Olivella, S., Gens, A., Carrera, J., and Alonso, E.E., 1996. Numerical formulation for a simulator (CODE-BRIGHT) for the coupled analysis of saline media. *Engineering Computations* **13**: 7, 87– 112.